Study of the triangular lattice tV model near $x=\frac{1}{3}$

O. I. Motrunich and Patrick A. Lee
Department of Physics, Massachusetts Institute of Technology, Cambridge, Massachusetts 02139
(Received 5 February 2004; published 22 July 2004)

We study the extended Hubbard model on a triangular lattice near doping $x=\frac{1}{3}$, which may be relevant for the recently discovered superconductor $Na_xCoO_2\cdot yH_2O$. By generalizing this model to N fermionic species, we formulate a meanfield description in the limit of large N. In meanfield, we find two possible phases: a renormalized Fermi liquid and a $\sqrt{3}\times\sqrt{3}$ charge density wave state. The transition between the two phases is driven by increasing the nearest-neighbor repulsion and is found to be first order for doping $x=\frac{1}{3}$, but occurs close to the point of the local instability of the uniform liquid. We also study fluctuations about the uniform meanfield state in a systematic $1/N$ expansion, focusing on the residual interaction of quasiparticles and possible superconducting instabilities due to this interaction. Upon moving towards the charge density wave instability, the increasing charge fluctuations favor a particular f-wave triplet state. (This state was recently discussed by Tanaka *et al.*, cond-mat/0311266.) We also report a direct Gutzwiller wave function study of the spin-$\frac{1}{2}$ model.

DOI: 10.1103/PhysRevB.70.024514 PACS number(s): 74.20.Rp

I. INTRODUCTION

Motivated by the recently discovered superconductivity[1] in $Na_xCoO_2\cdot yH_2O$ $\left(x\approx\frac{1}{3}\right)$ and the unusual electronic properties[2] of the Na_xCoO_2 series, we began a study of the tV model on a triangular lattice,[3] focusing primarily on the renormalized Fermi liquid regime. We pointed out that nearest-neighbor repulsion can lead to significant renormalization of the effective hopping amplitude, which seems to be the case in these materials. We also argued that strong repulsion drives this model into a $\sqrt{3}\times\sqrt{3}$ charge ordered state near commensurate dopings $x=\frac{1}{3}$ and $\frac{2}{3}$.

We continue this study here and perform a systematic slave boson meanfield analysis of the Fermi liquid close to the charge density wave (CDW) state for dopings near $x=\frac{1}{3}$. We also consider the residual interaction between the quasiparticles and study which superconductivity channels are favored in the tV model on the triangular lattice. Of particular interest here is the possible enhancement of some channels due to charge fluctuations upon approaching the CDW phase.

Such studies of superconductivity due to residual interaction in the models with strong local repulsion are familiar in the high-T_c field. Scalapino *et al.*[4] studied the Hubbard model on a three-dimensional cubic lattice in a random phase approximation (RPA) and found that d-wave pairing becomes attractive close to the spin density wave transition. Kotliar and Liu[5] studied the infinite-U Hubbard model on a two-dimensional square lattice in a systematic large-N treatment and found that the residual interaction from the no-double-occupancy constraint favors d-wave superconductivity close to half filling. More recently, McKenzie *et al.*[6] applied the analysis of Kotliar and Liu to the extended Hubbard model on the square lattice at a quarter filling and found a transition to the $\sqrt{2}\times\sqrt{2}$ CDW, which is driven by the nearest-neighbor repulsion. Merino and McKenzie[7] studied superconducting instabilities of the Fermi liquid near this transition.

It is of interest to perform similar studies on the triangular lattice. RPA treatment in the spirit of Scalapino *et al.*[4] has been done by Tanaka *et al.*[8] very recently. They find that in the regime of interest for $Na_xCoO_2\cdot yH_2O$, a particular f-wave triplet channel is favored close to the CDW instability.

Here, we report a Kotliar-Liu type analysis for the triangular lattice, which has not been done so far. The advantage of our approach over the RPA is that the treatment of the strong on-site repulsion is better controlled.

In our study, we also find that the preferred superconducting channel near the transition to the $\sqrt{3}\times\sqrt{3}$ CDW is the f-wave triplet state discussed by Tanaka *et al.*[8] This state has the lobes of large Δ oriented towards M points of the Brillouin zone (BZ) boundary as depicted in Fig. 1. The origin of this result can be understood from the following Fermi surface nesting argument.

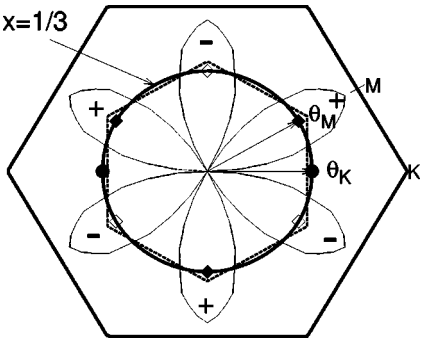

FIG. 1. Schematics of the nesting argument for doping $x=\frac{1}{3}$. External hexagon shows triangular lattice Brillouin zone, while internal hexagon shows reduced BZ for the $\sqrt{3}\times\sqrt{3}$ order. Flat surfaces of the reduced BZ boundary are connected by the $\sqrt{3}\times\sqrt{3}$ ordering wave vectors perpendicular to the surfaces. Near these momenta transfer, $V_{\text{eff}}(\theta,\theta')$ becomes attractive close to the CDW instability. We also show the f-wave triplet gap function that we find to be the dominant superconducting channel from the residual interaction; this channel utilizes the near nesting of θ_M points indicated with black diamonds.

In a RPA-type treatment, the effective interaction at wave vector q is

$$V_{\text{eff}}(q) = \frac{V(q)}{1 + 2\chi_0(q)V(q)}, \tag{1}$$

where $\chi_0(q)$ is positive. This can be also written as

$$V_{\text{eff}}(q) = V(q) - 2\chi(q)V(q)^2, \tag{2}$$

where $\chi(q) = \chi_0(q)/[1+2\chi_0(q)V(q)]$ is the full susceptibility in RPA. Now, $V(q)$ is negative over some portion of the BZ, in particular at the $\sqrt{3}\times\sqrt{3}$ ordering wave vectors such as $Q = 4\pi/(3a)\hat{x}$, so for sufficiently large V there is an instability at which $\chi(Q)$ diverges. Equation (2) shows that close to the instability the effective interaction becomes strongly attractive at the ordering wave vectors. If there are sections of the Fermi surface that are nearly connected by such wave vectors, then we expect enhanced superconductivity in channels that utilize this nesting. Our calculation using the slave boson theory also produces attractive effective interactions due to charge fluctuations. The difference is that now the effective potential depends on k and k' of the electrons, rather than $q = k - k'$. Near the Fermi surface we write this as $V_{\text{eff}}(\theta, \theta')$ and we find that V_{eff} has attractive components when θ and θ' are connected by an ordering vector Q.

Figure 1 shows the situation for doping $x = \frac{1}{3}$ (drawn to scale). It turns out that at this filling the Fermi surface lies fairly close to the reduced BZ corresponding to the $\sqrt{3}\times\sqrt{3}$ order. We also show the gap function Δ_k of the dominant f-wave state. This has large absolute values in the directions of the M points of the full BZ boundary and signs as shown—positive sign near black diamonds and negative sign for white diamonds. With an attractive $V_{\text{eff}}(Q)$, pairing between the black diamonds and also pairing between the white diamonds are very favorable, since the black diamonds are nearly connected among themselves by ordering wave vectors, and so are the white diamonds.

We should of course consider the near nesting of other Fermi surface segments as well. For example, take the point θ_K and the point opposite to it on the Fermi surface shown by the filled circles in Fig. 1. These points are also nearly connected by an ordering vector and this pairing would favor a spin singlet state. As an example, an s-wave state gains from all points θ, θ' that are connected by $V_{\text{eff}}(\theta, \theta') < 0$. The reason why the s-wave channel is still disfavored is that there remains significant overall repulsion over non-nested $V_{\text{eff}}(\theta, \theta')$ that it cannot avoid. The earlier f-wave state appears to be best for the overall V_{eff}.

The paper is organized as follows. We first perform a slave boson meanfield treatment of a generalized tV model with N fermion species. Near $x = \frac{1}{3}$, two candidate states are studied—a uniform Fermi liquid and a state with $\sqrt{3}\times\sqrt{3}$ charge order. The phase diagram is established. We then study fluctuations over the uniform saddle point in $1/N$ expansion, and focus on the residual quasiparticle interactions from such fluctuations. This approach can be viewed as a version of RPA that treats the on-site constraint systematically, and provides a more quantitative justification of the earlier nesting argument.

We conclude this Introduction with one remark. Earlier works[9–14] considered the tJ model on the triangular lattice and found that the dominant superconductivity from the J interaction is $d+id$ singlet state. This conclusion was also reached in our earlier report[3] in which we studied the tJV model and treated J as the main residual interaction. The tV model with no J terms predicts f-wave triplet state near the CDW order, and offers a way to distinguish between these two different pairing mechanisms. The experimental situation regarding the pairing symmetry of $Na_xCoO_2 \cdot yH_2O$ remains inconclusive, with controversy still surrounding whether there is a jump in the Knight shift below T_c.[15,16]

II. EXTENDED HUBBARD MODEL ON TRIANGULAR LATTICE

We consider the extended Hubbard model in the limit of large onsite repulsion, i.e., the following tV Hamiltonian

$$\hat{H}_{tV} = -P_G \sum_{ij} t_{ij} c_{i\sigma}^\dagger c_{j\sigma} P_G + \tfrac{1}{2}\sum_{ij} V_{ij} n_i n_j \tag{3}$$

with nearest-neighbor repulsion $V_{ij} = V$. P_G projects out double occupation of sites. The band is less than half filled, with the average fermion density of $1-x$ per site, and we specifically consider the case $t > 0$. See Refs. 3 and 9 for a more detailed discussion of the possible application of this Hamiltonian to the Na_xCoO_2 system. Here, we are primarily interested in the doping near $x = \frac{1}{3}$.

A. Meanfield formalism

Our meanfield treatment follows closely McKenzie *et al.*[6] The general formalism is the same except for an arithmetic difference in Eq. (14) and some minor differences in the analysis. We apply this formalism to the triangular lattice tV model. Slave boson formulation is used to treat the no-double-occupancy constraint. We write $c_{i\sigma}^\dagger = f_{i\sigma}^\dagger b_i$, and the slave boson Hamiltonian acts in the Hilbert space with $f_{i\sigma}^\dagger f_{i\sigma} + b_i^\dagger b_i = 1$; the boson field b keeps track of the empty sites.

To formulate a meanfield description and also in order to go beyond the meanfield in a systematic manner, we consider a generalized model with N fermionic species. The slave boson Hamiltonian is written as

$$\hat{H} = -\frac{1}{NS}\sum_{ij} t_{ij} f_{i\sigma}^\dagger f_{j\sigma} b_j^\dagger b_i + \frac{1}{2NS}\sum_{ij} V_{ij} f_{i\sigma}^\dagger f_{i\sigma}(NS - b_j^\dagger b_j), \tag{4}$$

which now acts in the space

$$f_{i\sigma}^\dagger f_{i\sigma} + b_i^\dagger b_i = NS \tag{5}$$

(the spin index σ runs from 1 to N). For convenience, we introduced parameter S, which is kept fixed as we take $N \to \infty$. We also used a particular form for the repulsion term. To study the system behavior with doping, we fix the total fermion number to $NS(1-x)$ fermions per site (our large N limit is thus like a thermodynamic limit in the fermion flavors). At the end of the calculation, we will put $N = 2$, $S = \frac{1}{2}$,

and our specific choices when defining H_{fb} are such that this will reproduce the slave boson Hamiltonian for the spin-$\frac{1}{2}$ model.

Proceeding as in McKenzie *et al.*[6] and Kotliar and Liu,[5] we write the path integral in the radial gauge[17]

$$Z = \int \mathcal{D}\bar{f}\mathcal{D}f\mathcal{D}r\mathcal{D}\lambda \exp\left[-\int_0^\beta d\tau \mathcal{L}(\tau)\right]. \tag{6}$$

The imaginary time Lagrangian

$$\mathcal{L} = \sum_i \bar{f}_{i\sigma}(\partial_\tau - \mu + i\lambda_i) f_{i\sigma} - \frac{1}{NS}\sum_{ij} t_{ij} r_i r_j \bar{f}_{i\sigma} f_{j\sigma} + \frac{1}{2NS}\sum_{ij} \bar{f}_{i\sigma} f_{i\sigma} V_{ij}(NS - r_j^2) + \sum_i i\lambda_i (r_i^2 - NS) + \mu \sum_i NS(1-x). \tag{7}$$

To obtain this, auxiliary field $\lambda_i(\tau)$ was introduced to enforce the constraint; the phase of the original boson field b_i was gauged away, while the absolute value is now a real field $r_i = |b_i|$ [the corresponding measure is $\mathcal{D}r = \Pi_{i,\tau} r_i(\tau) dr_i(\tau)$]. Chemical potential μ sets the correct fermion density.

We now formally integrate out the fermions and seek saddle points of the resulting action in terms of the fields r_i and λ_i. The natural scale for the r fields is $r^2 \sim N$, and upon such rescaling (which we do not perform explicitly) the saddle point analysis can be cast into a formal large N procedure.

The saddle point conditions read

$$\langle \bar{f}_{i\sigma} f_{i\sigma} \rangle + r_i^2 = NS, \tag{8}$$

i.e., the constraints are satisfied on average, and

$$\varphi_i \equiv i\lambda_i = \frac{1}{2NS}\sum_j \frac{r_j}{r_i}[t_{ij}\langle \bar{f}_{i\sigma} f_{j\sigma}\rangle + t_{ji}\langle \bar{f}_{j\sigma} f_{i\sigma}\rangle] + \frac{1}{2NS}\sum_j V_{ji}\langle \bar{f}_{j\sigma} f_{j\sigma}\rangle. \tag{9}$$

We seek time-independent saddle points. However, the fields may be spatially varying to allow for possible charge inhomogeneity. In this case, $\varphi_i + (1/2NS)\Sigma_j V_{ij}(NS - r_j^2)$ is an effective potential on site i [cf. Eq. (7)], while $(1/NS) r_i r_j t_{ij}$ is an effective hopping amplitude in such meanfield. Among all saddle points, we are to take the one that minimizes the free energy specified by Eq. (7).

We first consider the uniform saddle point, which has $r_i^2 \equiv b^2 = NSx$ and

$$i\lambda_i \equiv \varphi = \frac{1}{NS}\frac{N}{L^d}\sum_k \left(\tilde{t}_k + \tfrac{1}{2}\tilde{V}_0\right) f(\xi_k). \tag{10}$$

Here, $\tilde{t}_k = \Sigma_{r'} t_{rr'} e^{-ik(r-r')}$ and similarly for $\tilde{V}_k$ (we will often drop tildes when the meaning is unambiguous); L^d is the number of lattice sites; $f(\xi) = 1/(e^{\beta\xi}+1)$ is the Fermi distribution; and ξ_k is the quasiparticle energy measured relative to the Fermi level

$$\xi_k = -x\tilde{t}_k + \varphi + \tfrac{1}{2}\tilde{V}_0(1-x) - \mu. \tag{11}$$

The chemical potential is tuned so that

$$\frac{1}{L^d}\sum_k f(\xi_k) = S(1-x). \tag{12}$$

The uniform saddle point represents a renormalized Fermi liquid with effective hopping xt_{ij}. We recognize such hopping energy renormalization as coming from the configurational constraints imposed by the no-double-occupancy condition. At this level, the repulsive interaction leads only to the shift in the bottom of the band.

B. Fluctuations over the uniform state

Away from half filling and for small V, the uniform saddle point has the lowest free energy. We can establish the region of its local stability by considering small fluctuations above the uniform state. Proceeding as in Refs. 5 and 6, we obtain the following quadratic action for the fluctuations $i\lambda_i = \varphi + i\delta\lambda_i$, $r_i = b(1+\delta r_i)$:

$$S^{(2)} = \frac{1}{2}\sum_{q,\omega_n} [\delta r(-q,-\omega_n) \quad \delta\lambda(-q,-\omega_n)] \begin{pmatrix} \Gamma_{rr} & \Gamma_{r\lambda} \\ \Gamma_{\lambda r} & \Gamma_{\lambda\lambda} \end{pmatrix} \times \begin{pmatrix} \delta r(q,\omega_n) \\ \delta\lambda(q,\omega_n) \end{pmatrix}, \tag{13}$$

where ω_n is bosonic Matsubara frequency, and the "inverse RPA propagator" is given by

$$\Gamma_{rr}(q,\omega_n) = 2b^2\varphi - \frac{2b^2}{NS}\frac{N}{L^d}\sum_k \left(t_{k+q} + \frac{1}{2}\tilde{V}_0\right) f(\xi_k) - \frac{b^4}{(NS)^2}\frac{N}{L^d}\sum_k \frac{f(\xi_{k+q}) - f(\xi_k)}{i\omega_n + \xi_k - \xi_{k+q}}(t_k + t_{k+q} + V_q)^2, \tag{14}$$

$$\Gamma_{r\lambda}(q,\omega_n) = \Gamma_{\lambda r}(q,\omega_n) = i\left[2b^2 + \frac{b^2}{NS}\frac{N}{L^d}\sum_k \frac{f(\xi_{k+q}) - f(\xi_k)}{i\omega_n + \xi_k - \xi_{k+q}}(t_k + t_{k+q} + V_q)\right], \tag{15}$$

$$\Gamma_{\lambda\lambda}(q,\omega_n) = \frac{N}{L^d}\sum_k \frac{f(\xi_{k+q}) - f(\xi_k)}{i\omega_n + \xi_k - \xi_{k+q}}. \tag{16}$$

The above expressions coincide with Eq. (17) in Ref. 6 upon replacements $t/(NS) \to t/N$, $V/(NS) \to 2V/N$, except that the $\tilde{V}_0$ term in Γ_{rr} replaces $\tilde{V}_k$ there.

We can write more compactly

$$\Gamma_{rr} = \frac{2b^2}{NS}Y - \frac{b^4}{(NS)^2}(V_q^2 X_0 + 2V_q X_1 + X_2), \tag{17}$$

$$\Gamma_{r\lambda} = \Gamma_{\lambda r} = i\left[2b^2 + \frac{b^2}{NS}(V_q X_0 + X_1)\right], \tag{18}$$

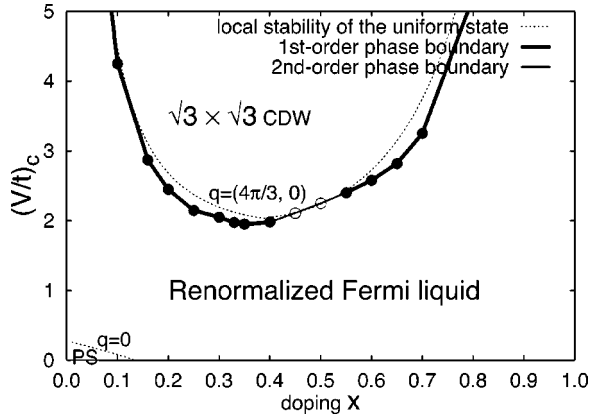

FIG. 2. Meanfield phase diagram of the tV Hamiltonian. For $x<0.14$, the uniform state is unstable at $q=0$ (towards phase separation) for small repulsion V, but is stabilized for moderate V. For large V, the instability occurs at the $\sqrt{3}\times\sqrt{3}$ ordering wave vector and the critical $(V/t)_c$ is shown with the dotted line. In the region between the dotted lines, the uniform state is locally stable at all wave vectors. The circles show the actual meanfield transitions with general $\sqrt{3}\times\sqrt{3}$ ansatz; filled circles indicate first-order phase transitions, while open circles indicate second-order transitions.

$$\Gamma_{\lambda\lambda} = X_0, \tag{19}$$

where we used Eq. (10) and introduced

$$X_p(q,\omega_n) = \frac{N}{L^d}\sum_k (t_k + t_{k+q})^p \frac{f(\xi_{k+q}) - f(\xi_k)}{i\omega_n + \xi_k - \xi_{k+q}}, \tag{20}$$

$$Y(q) = \frac{N}{L^d}\sum_k (t_k - t_{k+q}) f(\xi_k). \tag{21}$$

As discussed in Ref. 5, the local stability of the saddle point is determined by the condition $\det\Gamma = \Gamma_{rr}\Gamma_{\lambda\lambda} - \Gamma_{r\lambda}\Gamma_{\lambda r} > 0$, which translates to

$$X_0\left(\frac{4b^2}{NS}V_q + \frac{2Y}{NS} - \frac{b^2}{NS}\frac{X_2}{NS}\right) + b^2\left(2 + \frac{X_1}{NS}\right)^2 > 0. \tag{22}$$

We now focus on the stability to static perturbations, setting $\omega_n = 0$. Since $X_0 > 0$ and V_q is negative in some portion of the Brillouin zone, there is clearly an instability for sufficiently large V.

The local stability analysis specialized to $N=2, S=\frac{1}{2}$ (and in the zero-temperature limit) for all dopings is summarized in Fig. 2.

For $x<0.14$ there is an instability at $q=0$ for small V, which persists as long as

$$\det\Gamma(q=0) = \text{const}\times[1 + 2t_F\nu(\epsilon_F) + \tilde{V}_0\nu(\epsilon_F)] < 0, \tag{23}$$

where we used $X_0(q=0) = \nu(\epsilon_F)$, etc., $\nu(\epsilon_F)$ is the spinful density of states per site at the Fermi level. The instability is towards phase separation into hole-rich and hole-poor regions. This can be seen by examining the energy of the uniform state (measured per site)

$$H(x) = E_t(x) + \tfrac{1}{2}\tilde{V}_0(1-x)^2, \tag{24}$$

where $E_t(x)$ is the hopping energy per site in the free fermion problem with hopping amplitude tx and fermion density $(1-x)$. After some analysis, condition (23) is seen to be equivalent to $H''(x) < 0$, which indeed leads to phase separation. Note that moderate nearest-neighbor repulsion V stabilizes the uniform saddle point against phase separation, and the corresponding boundary is shown in the lower left hand corner of Fig. 2.

The instability of the uniform state for large V is found to always occur at the $\sqrt{3}\times\sqrt{3}$ ordering wave vector. The corresponding critical $(V/t)_c$ is shown with the dotted line in Fig 2. In the region designated renormalized Fermi liquid the uniform state is stable towards static fluctuations at any wave vector.

C. $\sqrt{3}\times\sqrt{3}$ CDW saddle points

However, local stability does not guarantee global stability of the saddle point. As a specific example, we consider $x=\frac{1}{3}$. The earlier local stability analysis gives

$$V_c(x = 1/3) = 2.11. \tag{25}$$

The uniform saddle point has the energy per site

$$E_{\text{uniform}}(x = 1/3) = -6tx\langle f^\dagger_{i\sigma} f_{j\sigma}\rangle + 3V(1-x)^2 \tag{26}$$

with $\langle f^\dagger_{i\sigma} f_{j\sigma}\rangle = 0.337$ for the uniform hopping at this doping.

On the other hand, consider a competing state with complete $\sqrt{3}\times\sqrt{3}$ order which has all charges on the B and C sublattices, $b_B = b_C = 0$, while the sublattice A is not occupied, $b_A = 1$. The energy per site is

$$E_{\sqrt{3}\times\sqrt{3}}(x = 1/3) = V. \tag{27}$$

It is simple to see that the latter becomes energetically preferred over the uniform state for $V=2.00$, i.e., below the local instability point of the uniform state, which means that the transition is first order. The following detailed analysis finds that the the actual transition occurs at $V_c^{\text{1storder}}(x=\frac{1}{3}) = 1.98$ to a state which is close to the above state with complete CDW order.

To study such possibilities in detail, we consider saddle points that have the $\sqrt{3}\times\sqrt{3}$ ordering pattern. The procedure is as follows: We select the A sublattice of the three sublattices, and seek saddle points that have $b_i = b_A$ on the A sublattice and $b_i = b_B = b_C$ on the B and C sublattices. Of course, these must satisfy $b_A^2 + b_B^2 + b_C^2 = 3x$. Similarly, we allow different φ_A and $\varphi_B = \varphi_C$. For convenience, we can take $\varphi_A + \varphi_B + \varphi_C = 0$, since there is also the chemical potential degree of freedom which is tuned to obtain the correct fermion density for each set b_A, φ_A. Now, for each b_A we tune φ_A until $b_A^2 + \langle f^\dagger_{A\sigma} f_{A\sigma}\rangle = 1$ is satisfied, and finally adjust b_A so that the other self-consistency condition Eq. (9) is satisfied. We find all such saddle points and compare their free energies obtained from Eq. (7). The result is shown in Fig. 2 with circles. Filled circles indicate the situation similar to $x=\frac{1}{3}$, when the transition is first order. For open circles, we tentatively conclude that the transition point coincides with that

determined by the local stability analysis and the transition is second order.

We considered in detail the uniform and the $\sqrt{3}\times\sqrt{3}$ CDW saddle points. Since we are interested in the doping regime near $x=\frac{1}{3}$, where we do not expect some other state to enter the competition, the presented meanfield analysis is complete.

III. RESIDUAL SUPERCONDUCTING INSTABILITIES

We now aim to go beyond the meanfield description. The free energy of the uniform state at next order in $1/N$ can be obtained from the quadratic action $S^{(2)}$, Eq. (13). In terms of the fermionic quasiparticles, this contains further effective mass renormalization as well as residual interaction of quasiparticles mediated by the bosons. We focus on the residual interaction, in order to decide which pairing channel is favored at low temperatures for our triangular lattice with hard repulsion.

The vertices coupling the fermions and the bosons can be obtained by examining the Lagrangian Eq. (7), while the boson propagators are given by the inverse of the matrix $\hat{\Gamma}(q,\omega_n)$ in the quadratic action, e.g., $D_{rr}(q,\omega_n)\equiv\langle\delta r(-q,-\omega_n)\delta r(q,\omega_n)\rangle=\Gamma_{\lambda\lambda}/\det\hat{\Gamma}$, etc. From the expressions for Γ and using $b^2\sim N$, all propagators are $O(1/N)$.

For our study, we single out interaction terms relevant for the Bardeen-Cooper-Schrieffer (BCS) instability, obtaining

$$V_{\rm eff}(k_1,k_2)=D_{\lambda\lambda}-\frac{b^4}{(NS)^2}D_{rr}|t_{k_1}+t_{k_2}+V_q|^2 + i\frac{b^2}{NS}[D_{\lambda r}(V_{-q}+t_{-k_1}+t_{-k_2}) + D_{r\lambda}(V_q+t_{k_1}+t_{k_2})], \quad (28)$$

where all boson propagators are at wavevector $q=k_1-k_2$. The interaction is of order $O(1/N)$. If we ignore the frequency dependence of the boson propagators, the relevant terms correspond to the standard pairing Hamiltonian

$$\hat{H}_{\rm pairing}=\frac{1}{2L^d}\sum_{k_1,k_2}V_{\rm eff}(k_1,k_2)f^{\dagger}_{k_1,\sigma}f^{\dagger}_{-k_1,\sigma'}f_{-k_2,\sigma'}f_{k_2,\sigma}. \quad (29)$$

From now on, we fix $N=2$, $S=\frac{1}{2}$. We first consider in detail doping $x=\frac{1}{3}$. We are primarily interested in the scattering processes when momenta k_1 and k_2 lie near the Fermi surface. Therefore, we visualize the effective interaction by fixing the momenta on the Fermi surface and plotting $V_{\rm eff}(\theta_1,\theta_2)$ as a function of polar angles. This is shown in Fig. 3, where we see how $V_{\rm eff}$ evolves for increasing V approaching the CDW transition. Observe that there is residual repulsion even when $V=0$, which is entirely due to the no-double-occupancy constraint, and that this repulsion already has some momentum space features. As we increase V from zero, the initial effect is to add more repulsion at zero momentum transfer. Increasing V further and approaching the $\sqrt{3}\times\sqrt{3}$ CDW instability, there is a dramatic development in the features associated with scattering at the $\sqrt{3}\times\sqrt{3}$ ordering wave vectors. As discussed in the introduction, the quasiparticle interaction at such momentum transfer becomes attractive close to the critical point, and this is clearly seen in the plots. In Fig. 3, the critical point $V_c=2.11$ is defined from the quadratic fluctuation analysis. As discussed earlier, in the meanfield, we find instead first-order phase transition at a somewhat lower $V_c^{\rm 1storder}=1.98$. However, the features in $V_{\rm eff}(\theta,\theta')$ are already enhanced at the actual transition since it occurs close to the instability point and has significant critical fluctuations, so we will mostly ignore the distinction in what follows.

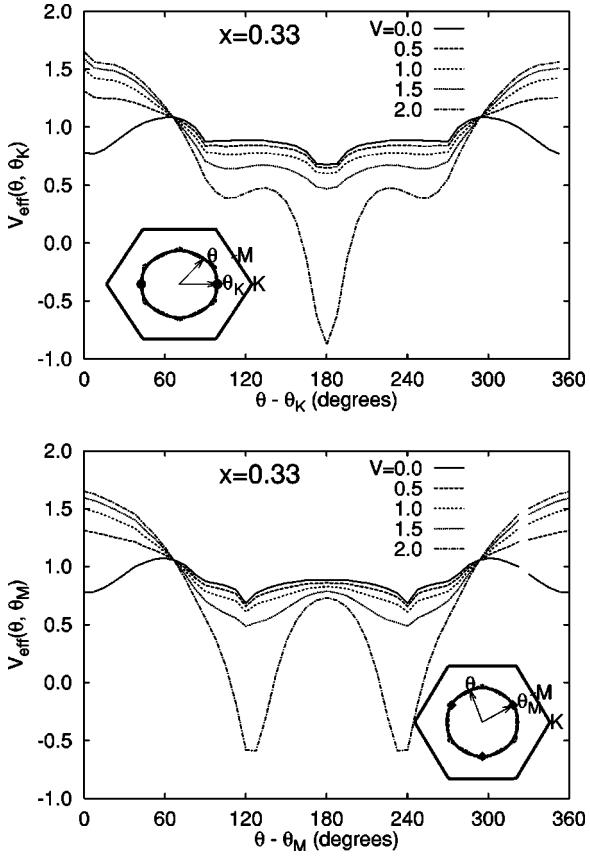

FIG. 3. Residual quasiparticle interaction relevant for the pairing instability [cf. Eq. (29)] plotted for the momenta k_1 and k_2 on the Fermi surface. One angle is kept fixed while the other is varied over the Fermi Surface as indicated in the insets, which also show the triangular lattice BZ and the reduced BZ for the $\sqrt{3}\times\sqrt{3}$ CDW order (see Fig. 1). The data are for $x=\frac{1}{3}$, and the uniform state becomes unstable at $V_c=2.11$. The vertical scale is in units of t. Top panel: The fixed angle is in the direction of the K point of the full BZ boundary. As we approach the CDW instability, 180° scattering amplitude becomes attractive, which is associated with the fact that the corresponding Fermi surface points (black circles) are nearly connected by one of the $\sqrt{3}\times\sqrt{3}$ ordering wave vectors. Bottom panel: The fixed angle is in the direction of the M point; the three nearly nested points occur at 120° from each other.

We now study BCS instabilities due to this residual interaction; the analysis below is valid for either singlet or $S_z=0$ triplet superconducting channels. We follow Refs. 4 and 5 and define coupling constant associated with each channel $\Delta_k\sim g_\alpha(k)$:

TABLE I. Triangular lattice harmonics evaluated in Fig. 4. e_1, e_2, $e_3=e_2-e_1$ refer to unit triangular lattice vectors. The labels are to be taken as descriptive only.

Ansatz g_k	Label
$\cos k\cdot e_1+\cos k\cdot e_2+\cos k\cdot e_3$	s
$\sin k\cdot e_2-\sin k\cdot e_3$	p_x
$\cos k\cdot e_2-\cos k\cdot e_3$	d_{xy}
$\sin k\cdot e_1-\sin k\cdot e_2+\sin k\cdot e_3$	f
$\sin k\cdot(e_1+e_2)-\sin k\cdot(e_2+e_3)+\sin k\cdot(e_3-e_1)$	NNN f
$\cos k\cdot(2e_1+e_2)-\cos k\cdot(e_1+2e_2)+\cos k\cdot(2e_2+e_3)$ $-\cos k\cdot(e_2+2e_3)+\cos k\cdot(2e_3-e_1)-\cos k\cdot(e_3-2e_1)$	i

$$c_\alpha=-\frac{\int\frac{d\sigma_k}{|v_k|}\int\frac{d\sigma_{k'}}{(2\pi)^d|v_{k'}|}g_\alpha(k)^*V_{\rm eff}(k,k')g_\alpha(k')}{\int\frac{d\sigma_k}{|v_k|}|g_\alpha(k)|^2}, \quad (30)$$

where the integration is over the Fermi surface elements $d\sigma$, and $v(k)=\nabla_k\xi(k)$ is the Fermi velocity. For an attractive channel, we must have $c_\alpha>0$, and the transitions temperature is given by the weak coupling BCS expression (which is appropriate in the present case)

$$T_c[\alpha]=\Omega\ \exp[-1/c_\alpha], \quad (31)$$

the frequency cutoff is roughly $\Omega\sim xt$, since the energy integration is over the entire band.

Representative triangular lattice tight binding harmonics that cover main symmetry classes are listed in Table I. Four of the ansatze have their real-space $\Delta_{rr'}$ nonzero on nearest-neighbor bonds only, the next-nearest-neighbor (NNN) f-wave ansatz has next-nearest-neighbor bonds, and the i-wave ansatz requires even further neighbor bonds. Since $V_{\rm eff}$ is real, only real ansatze need to be considered. Indeed, in this case the problem of finding a harmonic with the largest coupling constant is equivalent to a real symmetric eigenvalue problem; the easiest way to see this is to discretize the $d\sigma$ integrals and define $\psi_\alpha(k)=g_\alpha(k)(d\sigma_k/|v_k|)^{1/2}$.

Figure 4 shows the coupling constant c_α evaluated for the harmonics in Table I. We find that for all V (except very close to V_c) the NNN f-wave triplet is the dominant channel, while the other ansatze are repulsive or become repulsive upon increasing V. The performance of the NNN f-wave is understood by looking at the bottom panel of Fig. 2. The three marked points 120° from each other are nearly connected by $\sqrt{3}\times\sqrt{3}$ ordering wave vectors and the scattering among these points becomes attractive upon approaching the CDW regime. As displayed in Fig. 1, the NNN f-wave ansatz has its positive lobes oriented precisely in these three directions and is able to utilize this attraction.

Here, we note that generic next-nearest-neighbor ansatze utilize this nesting better than the nearest-neighbor ones, and we tried the corresponding NNN versions of the s, p, and d wave; the coupling constants are improved (not shown), but are still far from approaching the NNN f-wave ansatz. This is because each ansatz also has to pay the cost of repulsive scattering on large non-nested portions of the Fermi surface, and the NNN f-wave ansatz appears to be best here as well. For example, the coupling constant for the s-wave remains negative and appears on the scale of Fig. 4 only very close to the critical point, despite the fact that it gains from all attractive $V_{\rm eff}(\theta,\theta')<0$.

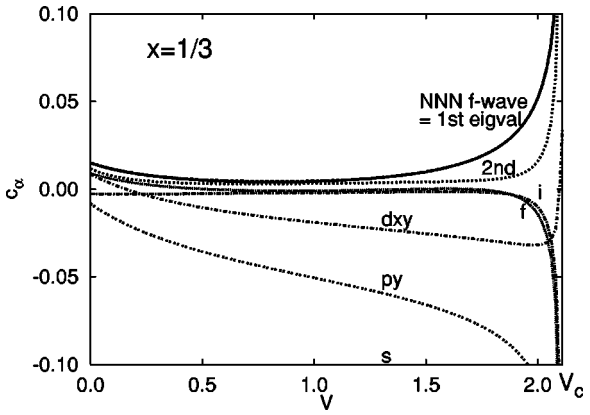

FIG. 4. Coupling constants for the triangular lattice harmonics in Table I (the s-wave ansatz is below the bottom of the plot). The doping is $x=\frac{1}{3}$, and the critical $V_c=2.11$ sets the right-hand plot boundary. We also show the maximal and the second eigenvalue; the NNN f-wave coupling constant coincides with the maximal eigenvalue for all V shown.

In fact, we also solve the full eigenvalue problem specified by Eq. (30), and plot the first (maximal) and the second eigenvalue in the same figure. We find that the NNN f-wave coupling constant coincides with the maximal eigenvalue in the entire range of $V<V_c$ (except maybe very close to V_c). The second eigenvalue is well separated from the first; the corresponding eigenvector over a large range of V does not have one of the simple s, p, d, or i character, but instead has eight lobes in momentum space, four of each sign.

Finally, Fig. 5 shows the maximal eigenvalue as a function of V for several dopings. In each case, the maximal eigenvalue corresponds to the NNN f-wave ansatz. The nesting displayed in the bottom panel of Fig. 3 that favors the

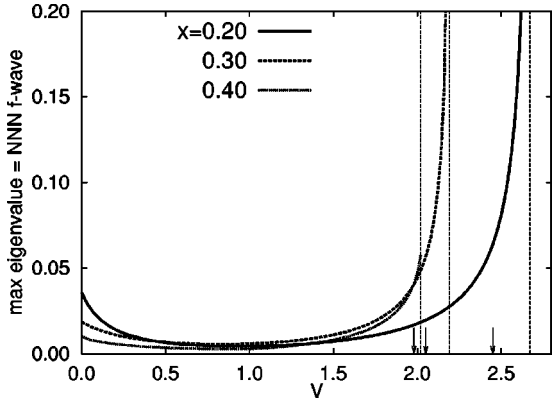

FIG. 5. Maximal eigenvalue for dopings $x=0.20$, 0.30, and 0.40. The critical V_c from the quadratic fluctuation analysis is indicated by vertical line in each case, while the first-order transition is indicated with the corresponding arrow near the bottom of the graph (cf. Fig. 2).

NNN f-wave improves as we lower the doping, since the Fermi surface passes through the end points of the reduced BZ when $x=0.194$ (see also Fig. 1). From Fig. 5 we see that the enhancement in the coupling constant is strongest and over the broadest range for $x=0.20$. Observe also that the residual interaction from the no-double-occupancy constraint only ($V=0$) also favors the discussed NNN f-wave channel on the triangular lattice.

We conclude by discussing what these results mean for the scale of superconductivity. We see that because of the nesting the maximal c_α can be relatively large compared to similar predictions in the non-nested cases (such as square lattice at finite doping, Ref. 5). However, if we use Eq. (31) literally, the obtained scale of T_c is still very small: for example, if we take $c_\alpha=0.1$, which is fairly large, then $\exp[-1/c_\alpha]\sim 5\times 10^{-5}$, which is tiny. Here we remark that one specific ingredient that can enhance T_c is missing in the present treatment, namely, the enhancement of the effective mass by the nearest-neighbor repulsion while remaining in the Fermi liquid. More precisely, at the presented level of analysis, the effective hopping $t_{\text{eff}}=xt$ is not renormalized by V, whereas it can become several times smaller when additional short-range correlations are included as discussed in Ref. 3 and in the following section. Since $1/c_\alpha \sim t_{\text{eff}}/V_{\text{eff}}$, this can have dramatic effect on the calculated T_c.

IV. JASTROW-GUTZWILLER WAVE FUNCTION STUDY—DISCUSSION

We now consider in some detail how the above results apply to the original spin-$\frac{1}{2}$ model. To this end, we have performed a systematic trial wave function study of the tV model. Specifically, we consider a family of Jastrow-Gutzwiller wave functions[3,18]

$$\Psi_{JG}(r_1\sigma_1,\dots)=e^{-\sum_{i<j}u(r_i-r_j)}\det[\psi_\alpha(R_j)]\det[\psi_\alpha(R'_j)], \tag{32}$$

where $\{R\}$ and $\{R'\}$ denote the positions of spin-up and spin-down fermions, respectively, and the wave function is nonzero only when the two sets do not overlap, which is the result of Gutzwiller projection. $\{\psi_\alpha\}$ refer to appropriate single-particle states that are occupied in the "preprojected" wave function. Each configuration of fermions is also weighted by a Jastrow factor defined via two-particle pseudopotentials $u(r_i-r_j)$, which puts additional correlations into the wave function.

The Fermi liquid state is obtained by occupying appropriate plane wave states ψ_k, $|k|\leqslant k_F$. From our studies of the tV model, we conclude that already the nearest-neighbor Jastrow factor gives good control over local correlations and is sufficient for an accurate energetics distinction between the Fermi liquid and competing charge ordered state.

As discussed at length in Ref. 3, lattice gas system described by the nearest-neighbor $u(r_i,r_j)\equiv W$ undergoes a transition to a $\sqrt{3}\times\sqrt{3}$ state for large W. Our direct optimization with such single-parameter wave function showed that this state is driven into the charge-ordered regime for sufficiently strong repulsion V and dopings in the range $0.27<x<0.50$. We also mentioned that once this happens, we are no longer justified in using plane waves for the preprojected orbitals. We should instead consider more general single-particle states; for example, we consider orbitals obtained by diagonalizing a "trial" Hamiltonian

$$\hat{H}_{\text{CDW}}=-\sum_{ij}\chi_{ij}c^\dagger_{i\sigma}c_{j\sigma}+\sum_i\varphi_i c^\dagger_{i\sigma}c_{i\sigma}, \tag{33}$$

where we allow generic hopping amplitudes χ_{ij} and site potentials φ_i that follow the $\sqrt{3}\times\sqrt{3}$ ordering pattern. Specifically, we select the A sublattice and take $\chi_{AB}=\chi_{AC}=1+\kappa$, $\chi_{BC}=1-\kappa$; $\kappa>0$ makes the hopping more dice-lattice-like, while $\kappa<0$ makes it more honeycomb-like. We also use the convention $\varphi_B=\varphi_C=-\varphi_A/2$ and vary φ_A. Observe that this structure of the trial Hamiltonian is suggested by the mean-field treatment of the Fermi liquid-CDW competition in Sec. II, and in fact by any such meanfield. However, our wave functions have further local correlations built in by the Jastrow factors which allow the liquid to better accommodate the nearest-neighbor repulsion (also leading to significant renormalization of the bandwidth as discussed in Ref. 3), while this is missing in the meanfield.

We summarize our wave function studies for three dopings $x=0.24$, 0.33, and 0.40. We report only the result of the three-parameter W,κ,φ_A optimization. When $\kappa=0,\varphi_A=0$, we obtain the Fermi liquid state. As discussed earlier, this restricted study should suffice for an accurate determination of the uniform liquid to CDW transition.

For dopings $x=0.33$ and 0.40, we find rather abrupt transitions to the $\sqrt{3}\times\sqrt{3}$ state at $V_c(x=0.33)\approx 3.5$ and $V_c(x=0.40)\approx 4.0$. On the other hand, for the doping $x=0.24$, the system shows no ordering till very large $V=15$ to 20 and maybe even higher. Comparing with Fig. 2, the behavior at this lowest doping is very different from the meanfield prediction. This is an extreme manifestation of the fact that the charges are able to effectively avoid each other and remain in the liquid state, which is captured by our Jastrow-Gutzwiller wave function, while the meanfield uniform state cannot accommodate this and pays large repulsion energy cost.

Finally, having established the dominant local energetics, we also tried adding superconducting correlations on top of the renormalized Fermi liquid state. We tried several superconducting ansatz including extended s wave, $p+ip$, $d+id$, f wave, and also their NNN versions. However, in our studies we were not able to detect any improvement in the energetics upon adding superconductivity. From this we conclude that if some such state appears at low energies, the condensation energy is still very small to be detected by direct numerical studies. In this situation, we are left to rely on approximate analytical calculations such as discussed in the main body of this paper.

ACKNOWLEDGMENTS

The authors thank Stuart Brown for bringing Ref. 7 to our attention. This work was supported by the National Science Foundation under Grant No. DMR-0201069. O.I.M. also wants to thank his family for support during his stay in Ukraine.

[1] K. Takada *et al.*, Nature (London) **422**, 53 (2003).
[2] I. Terasaki, Y. Sasago, and K. Uchinokura, Phys. Rev. B **56**, R12 685 (1997).
[3] O. I. Motrunich and P. A. Lee, cond-mat/0310387.
[4] D. J. Scalapino, E. Loh, and J. E. Hirsch, Phys. Rev. B **35**, 6694 (1987).
[5] G. Kotliar and J. Liu, Phys. Rev. Lett. **61**, 1784 (1988).
[6] R. H. McKenzie, J. Merino, J. B. Marston, and O. P. Sushkov, Phys. Rev. B **64**, 085109 (2001).
[7] J. Merino and R. H. McKenzie, Phys. Rev. Lett. **87**, 237002 (2001).
[8] Y. Tanaka, Y. Yanase, and M. Ogata, cond-mat/0311266.
[9] G. Baskaran, cond-mat/0306569.
[10] G. Baskaran, Phys. Rev. Lett. **91**, 097003 (2003).
[11] B. Kumar and B. S. Shastry, Phys. Rev. B **68**, 104508 (2003).
[12] Q.-H. Wang, D.-H. Lee, and P. A. Lee, Phys. Rev. B **69**, 092504 (2004).
[13] M. Ogata, J. Phys. Soc. Jpn. **72**, 1839 (2003).
[14] C. Honerkamp, Phys. Rev. B **68**, 104510 (2003).
[15] T. Waki, C. Michioka, M. Kato, K. Yoshimura, K. Takada, H. Sabarai, E. Takayama-Muromachi, and T. Sasaki, cond-mat/0306036; K. Yoshimura (private communication).
[16] Y. Kobayashi, M. Yokoi, and M. Sato, J. Phys. Soc. Jpn. **72**, 2453 (2003).
[17] N. Read and D. M. Newns, J. Phys. C **16**, 3273 (1983).
[18] D. M. Ceperley, G. V. Chester, and M. H. Kalos, Phys. Rev. B **16**, 3081 (1977).